JACS Au
AN OPEN ACCESS JOURNAL OF THE AMERICAN CHEMICAL SOCIETY

pubs.acs.org/jacsau
Article

Generalized Model for Inhibitor-Modulated 2D Polymer Growth to Understand the Controlled Synthesis of Covalent Organic Frameworks

Shubhani Paliwal,[⊥] Wei Li,[⊥] Pingwei Liu,* and Ananth Govind Rajan*

Cite This: https://doi.org/10.1021/jacsau.4c00077
Read Online

ACCESS | Metrics & More | Article Recommendations | Supporting Information

ABSTRACT: Two-dimensional (2D) polymers, also known as 2D covalent organic frameworks (COFs), are increasingly finding use in applications such as membrane separations, catalysis, and energy conversion. Current research is focused on the development of new synthesis routes for COFs and obtaining a mechanistic understanding of the growth process to control it in a better manner. In this regard, synthesis methods such as reversible polycondensation termination use monofunctional inhibitor species to achieve a controlled growth rate for COFs. However, so far, the role of the inhibitors in modulating the kinetics of COF growth is inadequately understood. In this work, inspired by the Mayo−Lewis framework, we develop a generalized kinetic model to describe the synthesis of a 2D COF monolayer. Our model involves six parameters corresponding to the rate constants of attachment and detachment of monomer and inhibitor species, as well as enhancement factors that quantify the effect of the local coordination environment of the attaching/detaching species on the reaction kinetics. We measure the inhibitor concentration-dependent growth kinetics of the COF experimentally and fit our model to experimental yield data, with the same parameters working across multiple inhibitor concentrations. As the growth process is inherently stochastic, we use this knowledge to develop a comprehensive kinetic Monte Carlo (KMC) simulation of 2D COF synthesis, demonstrating that scaled rate constants are required in the inherently *local* KMC simulations rather than those obtained from the *global* kinetic model. The KMC simulations point to an inverse flake size−inhibitor concentration relationship, in agreement with experiments, indicating that flake sizes could be precisely regulated by changing the inhibitor concentrations. Overall, our work promises to improve the understanding of 2D COF synthesis and will help in controlling the growth process to obtain the desired flake size distribution and product morphology.

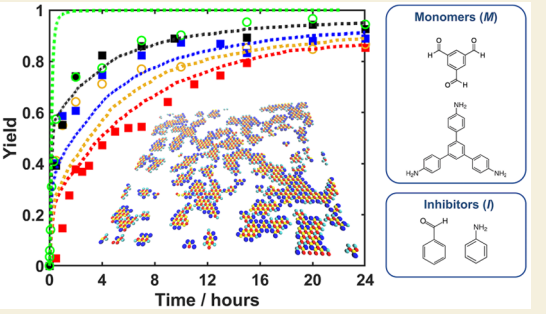

KEYWORDS: *COF, 2D polymers, kinetic model, KMC, polymer structure, growth mechanism*

INTRODUCTION

Two-dimensional (2D) polymers are a class of nanostructures that emerge from the linking of monomeric building units in two dimensions.[1,2] Variations in the linking mode between such building blocks lead to different kinds of structures such as covalently linked[3,4] and coordination polymers.[5] 2D covalent organic frameworks (COFs)[6] are an emerging class of crystalline, organic 2D polymer materials that are produced by the strong covalent linking between monomers. Due to their large surface area,[7] high extent of porosity,[4] and structural versatility,[8,9] 2D COFs find use in a wide range of applications,[10−14] including gas separation and storage,[15,16] catalysis,[17] energy conversion,[18] and biotechnology.[19] The factors that affect the shape and the pore sizes of the 2D COFs are the monomers' geometry and dimensions. Moreover, the lateral extent of crystallinity in COFs can be enhanced from a few nanometers to the micrometer scale by controlling their nucleation and growth. Previously, Bredas, Ditchel, and co-workers pioneered the development of models for the synthesis of COFs.[20−23] These studies provided new insights into the nucleation−elongation dynamics and the anisotropic growth of 2D COFs. However, there is presently no generalized theory that includes the effect of the functionalities (i.e., coordination numbers) of the monomeric species while describing the synthesis of 2D COFs, forming a knowledge gap in the field. Accounting for all possible bonded configurations of monomers is important in a modeling framework, particularly because the dynamics of 2D COF growth is dictated by the number of free bonding sites available in the reacting monomers. Accordingly, this work is aimed at addressing the above-mentioned gap by developing a comprehensive theoretical and simulation framework to model the controlled growth of 2D COFs considering

Received: January 24, 2024
Revised: April 28, 2024
Accepted: May 3, 2024
Published: May 31, 2024

two different inhibitors and two trifunctional monomers which can exhibit functionalities ranging from zero (in a free monomer) to three (in a fully bonded monomer).

Several techniques[24] can be used to synthesize high-crystallinity COF structures, such as two-step reaction pathways,[25] reversible reactions,[26] and preorientation of monomers.[27] Among these, the synthesis of COFs by the reversible bond formation method is the preferred one for obtaining high crystallinity. This approach is based on dynamic covalent chemistry,[28] i.e., obtaining polymers from a pool of monomers by continuous bond formation and breakage. As the reaction of monomers with each other is rapid and the products precipitate immediately, the reversible reactions enable morphology control by avoiding kinetic traps.[29] Introducing monofunctional competitors in the reaction system to reversibly inhibit the attachment of monomers is a viable method to control COF growth kinetics by slowing down polymerization, thus leading to products with good crystallinity and excellent thermal stability. Indeed, the COFs obtained using this approach only begin to decompose over 400 °C, as discussed in previous work.[30] Note that in this work, we use the terms inhibitors and competitors interchangeably as these molecules compete for attachment to the edge sites of the COF and thus inhibit its growth in a controlled manner.

Several research studies have been conducted to control the properties of COFs at the micro/macro scales to enhance their applications in various fields.[22,29,31−35] Smith et al.[29] experimentally explored the growth of imine-linked 2D COFs, which revealed the rapid formation of an amorphous network. Tianqiong et al.[31] used excess aniline in the reaction system to synthesize large-area single crystals of imine-based 3D COFs. In another study, Chen et al.[35] synthesized crystalline COF mesocrystals (nanocrystals with a common crystallographic orientation) by adding an alkyl amine as a modulator to a trifunctional monomer, which led to the growth of a uniform COF structure. Further, Zhao et al.[34] used a monofunctional amine as a competitor to synthesize crystalline COF aerogels with a controlled diameter. Recently, Wang et al.[30] introduced a reversible polycondensation termination method to generate higher-order COF structures by adding two monofunctional competitors simultaneously in the reaction system. However, a precise understanding of how the competitors regulate the nucleation and growth process at the molecular level remains elusive. Thus, theoretical studies are necessary to delineate the reaction mechanism and to use this knowledge to control the morphology of the COFs.

In this regard, kinetic Monte Carlo (KMC) simulations offer a robust framework to study the nucleation and growth of 2D materials.[21,36,37] Since the growth of COFs takes place in the solution phase and involves several monomeric and inhibitor species, one needs to account for these processes within a KMC framework. To this end, Li et al.[21] reported a KMC simulation to study the formation of a boronate ester-linked COF to control the nucleation rate, leading to enhancement of the material's quality. In their group's subsequent work,[23] one monofunctional competitor was introduced, which suppressed nucleation and enabled seeded growth polymerization that led to the controlled synthesis of a 2D COF. In another study, Nguyen et al.[38] investigated the reasons for the poor crystallinity of COF-5 (a 2D COF formed by condensation reactions) using molecular dynamics simulations. When the stacking interactions between the aromatic molecular constituents were weakened, leading to a slow aggregation rate, structures with increased crystallinity were observed. However, before the stacking of COF layers can be modeled, one needs to understand the formation of a single COF layer. To this end, a detailed theoretical model of monolayer COF growth that considers monomeric species with various functionalities, which can extract the COF growth rate constants from experimental data, can be particularly valuable.

Accordingly, in this work, we develop a generalized framework to model the synthesis of 2D COFs using a theoretical approach inspired by the well-known Mayo−Lewis model,[39] as well as KMC simulations. The model developed here is generalized in the sense that it can be applied to the synthesis of 2D COFs using monomers with any number of functionalities. Although the current model makes use of first-order reaction kinetics for modeling polymerization, higher-order kinetics can be readily incorporated. We measure the time dependence of the COF yield experimentally and use it to determine the kinetic model parameters. Note that the application of this model to other 2D polymers would simply involve refitting the model parameters. We primarily focus on unraveling the role of competitors in regulating the COF growth process as well as their effect on the 2D flake size. This is akin to how the molecular weight of polymeric chains is regulated by using monofunctional inhibitors during linear polycondensation of bifunctional monomers. To simplify the model, we neglect the stacking and aggregation of the 2D COF layers in three dimensions.

Our 2D COF reaction system consists of two trifunctional monomers, 1,3,5-benzene-tri carbaldehyde (BTCA) and 1,3,5-tris (4-aminophenyl) benzene (TAPB), as well as two monofunctional competitors, aniline and benzaldehyde. As the first step, we develop a comprehensive theoretical model based on unified reaction parameters for the system that can describe various scenarios where the inhibitors are present in different proportions to the monomers. Next, we determine the temporal variation of the yield of the 2D polymer experimentally with varying amounts of inhibitors in the reaction system. By fitting the rate constants in the model to the experimental yield vs time data, we show that the model captures the regulatory mechanism by which the inhibitors modulate the growth rate of the COF. Subsequently, these rate constant values are used in a KMC simulation to predict the time evolution of the COF structure. We find that scaled rate constants are required in the inherently *local* KMC simulations rather than those obtained from the *global* kinetic model to match the experimental yield vs time data. Interestingly, the KMC simulations reveal an inhibitor concentration−flake size trade-off, whereby higher inhibitor concentrations can bring in more control in the COF growth process but can reduce the resultant flake size. Overall, our work presents and validates a generalized theoretical model for describing the inhibitor-modulated synthesis of 2D COFs.

RESULTS AND DISCUSSION

Generalized Mechanistic Model of COF Synthesis

We began by developing a theoretical model to describe the steps involved in the polycondensation reaction mechanism with BTCA (M_1) and TAPB (M_2) as the monomers. The inhibitors present in the system are benzaldehyde (I_1) and aniline (I_2). Our reaction network is inspired by the seminal Mayo−Lewis theory[39] of polymerization from 1944 and is presented in Table 1. Some of our assumptions are also derived from that work, e.g., equal activities of a given functional group irrespective of its neighboring chain constituents and no effect of

https://doi.org/10.1021/jacsau.4c00077
JACS Au XXXX, XXX, XXX−XXX

Table 1. Reactions Involved in the Generalized Mechanistic Model for the Synthesis of 2D COFs Involving Monomers M_1 and M_2 and Inhibitors I_1 and I_2[a]

reaction type	
inhibitors attaching to monomers	
$M_1^x + I_2 \rightleftharpoons M_1^x$	(1)
$M_2^x + I_1 \rightleftharpoons M_2^{y-1}$	(2)
polymer growth	
$M_1^x + M_2^y + a_1P_1^1 + a_2P_1^2 + b_1P_2^1 + b_2P_2^2 \rightleftharpoons P_1^{x-1-b_1-b_2} + P_1^{y-1-a_1-a_2} + a_1P_1^0 + a_2P_1^1 + b_1P_2^0 + b_2P_2^1$	(3)
$M_1^x + b_1P_2^1 + b_2P_2^2 \rightleftharpoons P_1^{x-b_1-b_2} + b_1P_2^0 + b_2P_2^1$	(4)
$M_2^y + a_1P_1^1 + a_2P_1^2 \rightleftharpoons P_2^{y-a_1-a_2} + a_1P_1^0 + a_2P_1^1$	(5)
inhibitors attaching to COF	
$P_1^x + I_2 \rightleftharpoons P_1^{x-1}$	(6)
$P_2^y + I_1 \rightleftharpoons P_2^{y-1}$	(7)
inhibitor condensation	
$I_1 + I_2 \rightleftharpoons I_1I_2$	(8)

[a] x and y denote the number of free bonds in a species. Monomers that are part of the polymer are denoted as P_1 and P_2. Parameters a_1, a_2, b_1, and b_2 are stoichiometric coefficients of the polymeric units *adjacent* to the incoming monomers and quantify the local coordination environment of the attaching monomeric units. Note that water molecules are excluded from the reactions shown here.

penultimate groups. Nevertheless, we do incorporate the effect of neighboring species from the perspective of the monomer getting added to the COF, via the use of an enhancement factor (see below). The set of reactions are divided into four categories in our mechanistic model. The first set consists of the reactions corresponding to the addition of an inhibitor to a monomer, as given by reactions 1 and 2 in Table 1. The second set of reactions in Table 1 corresponds to the reactions leading to the growth of the COF, which either involves the reaction of two monomers to form a dimer that bonds with the COF or involves the direct attachment of M_1 or M_2 to any free end of the COF directly, as represented by reactions 4 and 5, respectively, in Table 1. The third set of reactions in Table 1 is inhibitor addition to the COF, as represented by reactions 6 and 7. The fourth and final type of reaction is the condensation of inhibitors to form an imine. Note that M_1^x represents the trifunctional monomer BTCA with x free bonds so that the range of x is [0,3]. Similarly, y represents the number of free bonds of the trifunctional monomer M_2^y. When an inhibitor attaches to a monomer, the number of free bonds of the monomer reduces by one. In the case of deattachment of an inhibitor from a monomer, the number of free bonds of M increases by one. Since a maximum of three inhibitors can attach to a monomer as there are three free bonds, the monomer BTCA can be present in the forms M_1^3, M_1^2, M_1^1, and M_1^0 in the reaction mixture.

We present pictorial representations of some example reactions in Figure 1A–B (reaction types 2 and 6) and Figure 1C (reaction type 3). In Figure 1A,B, we present schematics of the inhibition reactions involving monomeric and polymeric species, respectively. Figure 1A depicts an example of reaction type 2, which involves the attachment of inhibitor I_1 to monomer M_2^1, which has only one free bond, to give M_2^0. Figure 1B provides an example of reaction type 6. Therein, inhibitor I_2 attaches to polymer P_1^1 to give P_1^0, which has zero free bonds as two bonds are occupied by inhibitors and one bond is attached with the rest of the COF. Finally, one example of complex polymer growth (reaction type 3) is shown in Figure 1C. Here, the monomeric species M_1^3 and M_2^2 react to form a dimer and further attach to the free ends of the COF (P_1^1, P_2^2, and P_2^1, in the example).

The rate for reaction 1 can be calculated as $k_i[M_1^x][I_2]$ and that for the backward reaction can be calculated as $k_{ir}[M_1^{x-1}]$, where the square brackets represent the activity of the species. k_i and k_{ir} are reaction rate constants for inhibitor attachment and detachment reactions, respectively. In this work, we use the species molarity as the activity of each species. Other possible choices of activity, such as the mole fraction, can be explored in future work. We ignore changes in the solution volume as we use only 0.05 mmol of monomers, which would correspond to a water volume of 2.7 μL produced when considering a 3:1 ratio of water produced to monomers reacted upon condensation and assuming all the monomers to have reacted. This change is negligible compared to the volume of the solution (~10.1 mL, see Methods). Even accounting for the production of water during the imine condensation reaction in the 12C case, only 10.8 μL of water is produced when all the monomers are consumed, thus indicating the negligible role played by water formation in changing species concentration in this work. Following a similar procedure, reaction rate expressions are obtained for reaction 2. The second set of reactions in Table 1 corresponds to the reactions leading to the growth of the COF, which can occur through two routes. First, two monomers, M_1 and M_2, can react with each other to form a dimer that bonds with the COF, as represented by reaction 3 in Table 1. In this reaction (see Figure 1C for an example), P_1^1 represents a free end of the polymer which is formed by M_1, and it has one free bond, while P_1^2 can form two new bonds. a_1 and a_2 represent the number of available P_1^1 and P_1^2 neighbors, respectively, to which the dimer can attach. Note that P_1^0 has no free bonds. Analogously, b_1 and b_2 represent the number of available P_2^1 and P_2^2 neighbors. Again, P_2^0 has no free bonds. Upon attachment to M_2^y, b_1 units of P_2^1, and b_2 units of P_2^2, the M_1^x converts to $P_1^{x-1-b_1-b_2}$. Similarly, the M_2^y converts to $P_2^{y-1-a_1-a_2}$ upon forming a dimer and getting incorporated into the COF network. Now, certain conditions need to be imposed on the maximum number of $P_1^{\{1,2\}}$ and $P_2^{\{1,2\}}$ to which the dimers can attach. For example, if M_1 has two free bonds (i.e., $x = 2$), it can only attach to one P_2^1 or P_2^2 as its one free end will be used to bond with M_2 to form a dimer. This shows that the sum of b_1 and b_2 must always be strictly less than x for this type of reaction to take place. An analogous rule applies to a_1 and a_2 as well, whereby the sum of a_1 and a_2 must be strictly less than y.

We also included an enhancement factor F_f for the attachment of monomers and a de-enhancement factor F_b for their detachment in the calculation of reaction rates in our model to account for the effect of the coordination environment on the growth process. Accordingly, when a monomer or a dimer attaches to more than one P_1 or P_2, the rate constant of the reaction is enhanced by the factor F_f raised to the power of the number of neighbors it is attaching to, as given by the expression $k_mF_f^{a_1+a_2+b_1+b_2}$. Here, k_m denotes the rate constant for the forward reaction when a monomer attaches to another monomer or to the COF. This is because the rate of monomer or dimer attachment should be higher when it forms more than one new bond with the COF as the activation energy barrier decreases as per the well-known Evans–Polanyi relationship (linear relationship between the activation barrier and the reaction energy). The rate expression for reaction 3 is thus $k_mF_f^{a_1+a_2+b_1+b_2}[M_1^x][M_2^y]$

https://doi.org/10.1021/jacsau.4c00077
JACS Au XXXX, XXX, XXX–XXX

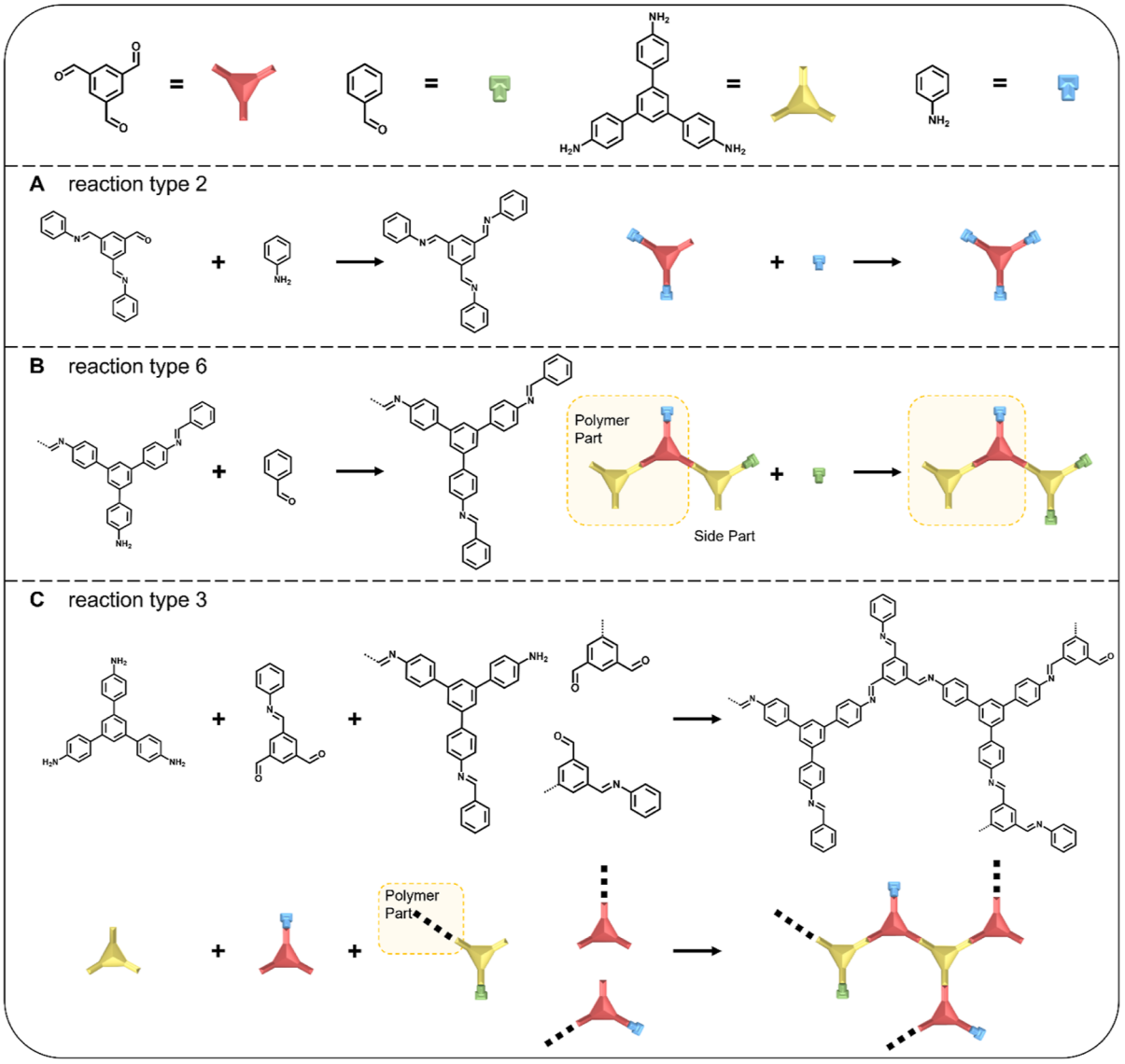

Figure 1. Examples of various chemical reactions in the mechanistic model. (A) Example of an inhibitor attachment to a monomer ($M_2^1 + I_1 \rightarrow M_2^0$; reaction type 2 in the model). (B) Example of an inhibitor attachment reaction to a polymer ($P_1^1 + I_2 \rightarrow P_1^0$; reaction type 6 in the model). (C) Schematic of a polymer growth reaction ($M_1^3 + M_2^2 + 1P_1^1 + 1P_2^2 + 1P_2^1 \rightarrow P_1^0 + P_2^0 + 1P_1^0 + 1P_2^1 + 1P_2^0$; reaction type 3 in the model). Dashed black lines depict bonds with the rest of the COF.

$[P_1^1]^{a_1}[P_1^2]^{a_2}[P_2^1]^{b_1}[P_2^2]^{b_2}$. Similarly, when a monomer detaches from the COF after it was attached with more than one bond to the COF, the tendency of this reaction decreases by the factor F_b raised to the number of neighbors it is attached to. Thus, one can write the rate constant expression for the reverse reaction corresponding to reaction type 3 as $k_{mr}F_b^{-(a_1+a_2+b_1+b_2)}$, where k_{mr} denotes the rate constant for the detachment of a monomer from another monomer or from the COF.

The second route for polymer growth is when either M_1 or M_2 attaches to any free end of the COF directly, as represented by reaction types 4 and 5 in Table 1. While calculating the rate for these reactions, the enhancement factor F_f is raised by the exponent of one less than the number of neighbors the monomer is attaching to. The reason is that the base rate constant, k_m, already includes the formation of one bond with the COF (note that for reaction type 3, this is not applicable because the bond between the M_1 and M_2 species needs to be accounted for). Thus, the rate constant expressions for monomer attachment and detachment are $k_m F^{b_1+b_2-1}$ and $k_{mr}F_b^{-(b_1+b_2-1)}$, respectively. Accordingly, the rate expression for forward reaction type 4 can be written as $k_m F_f^{b_1+b_2-1}[M_1^x][P_2^1]^{b_1}[P_2^2]^{b_2}$. The rate expressions for reverse reaction types 4 and 5 and forward reaction type 5 are obtained in a similar manner. As discussed later, we estimate the enhancement factor F_f and the de-enhancement factor F_b along with the rate constants k_m, k_{mr}, k_i, and k_{ir}. The third set of reactions in Table 1 is inhibitor addition to the COF, as represented by reactions 6 and 7. The rate expressions for the inhibitor attachment and detachment in reaction 6 are $k_i[P_1^x][I_2]$ and $k_{ir}[P_1^{x-1}]$, respectively. The rate expressions for reaction 7 can be obtained in a similar manner. Finally, we also consider the condensation of inhibitors to form an imine in our model. The last reaction is thus inhibitor (I_1 and I_2) condensation to form the imine I_{12}. The rate expressions for the forward and backward reactions are $k_i[I_1][I_2]$ and $k_{ir}[I_{12}]$, respectively. Note that the water generated in the reaction has almost no effect on the synthesis process (see Section S1 in the Supporting Information) in our experiments, so its concentration is neglected in the model. This follows from the small amount of

https://doi.org/10.1021/jacsau.4c00077
JACS Au XXXX, XXX, XXX−XXX

water produced in the system and forms an assumption that may be relaxed in future work. Meanwhile, the condensation product N-benzylideneaniline (I_{12}) showed the same effect as the individual inhibitors, indicating that imine exchange is possible and could be another important regulatory pathway. This inspires us to use N-benzylidene aniline instead of aniline and benzaldehyde as an inhibitor in future studies.

It is important to highlight that though the Mayo−Lewis approach is used as an inspiration for our model, the basic structure and assumptions differ in the development of our model and reaction system. Reversibility of copolymerization reactions is not considered in the Mayo−Lewis equation, which is taken into account in our model using the reaction rate constant k_{mr}. In the Mayo−Lewis system, reactions between the same two monomers to form homopolymers or block copolymers is possible. However, in our model, homopolymerization is not allowed and only an alternating polymer can be synthesized. Finally, in the Mayo−Lewis model, the reaction rate constants for M_1 attachment to P_y^2 and M_2 attachment to P_x^1 are taken to be different (k_{12} and k_{21}). On the contrary, in our model, both the rate constants are taken to be the same, i.e., k_m, to avoid too many parameters. Future work can explore the effect of different sets of assumptions on the 2D COF growth model.

Obtaining the Parameters in the Model by Fitting to Experimental Data

We used nonlinear least-squares data fitting via the lsqnonlin function in MATLAB R2022b to obtain the optimized values of the rate constants k_m, k_{mr}, k_i, and k_{ir}, the enhancement factor F_f, and the de-enhancement factor F_b. Experimental yield vs time data was measured at various inhibitor concentrations (see the Methods section) and was used to fit the model parameters. Plots of the experimental yield vs time are shown using various symbols in Figure 2, wherein filled squares depict data used to fit the model and unfilled circles represent data used to validate the model predictions. Note that theoretical studies were done in this work for the cases wherein the inhibitor concentration at the beginning is 3, 6, 9, and 12 times the initial concentration of both the monomers, considering that higher concentrations of inhibitors could significantly affect the thermodynamic equilibrium in the system, as shown in our previous work;[30] see below for further discussion on this point. These cases are referred to as 3C, 6C, 9C, and 12C, respectively. Experimental data regarding 0C (before 2 h) and 12C cases (all times) were already presented in ref 30 and are adapted from there. As seen in Figure 2, the higher the concentration of the inhibitors, the lower the yield at a given point in time during the reaction. We also verified this to be true using turbidity measurements,[40] as seen in the Supporting Information, Section S2, wherein the rate of growth of the COF is lower for higher inhibitor concentrations. A coupled system of ordinary differential equations involving the reaction rate expressions was solved to calculate the time evolution of the concentrations of each species. There are a total of 17 species in our reaction system: four each pertaining to monomers 1 and 2 (M_j^3, M_j^2, M_j^1, and M_j^0, where $j\in\{1,2\}$), two for the inhibitors involved (I_1 and I_2), one for the imine I_{12}, and three each for the polymer COF (P_j^2, P_j^1, and P_j^0, where $j\in\{1,2\}$). The root mean squared error between the predicted and the experimental yield was minimized to obtain the optimal parameters for the kinetic model. The bounds were set as zero to infinity for all the parameters while solving this optimization problem.

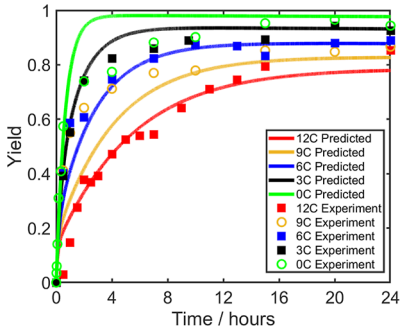

Figure 2. COF yield obtained from the kinetic model, as a function of time, for different amounts of inhibitors in the system. The symbols represent the experimental data and the solid lines represent the best-fit model predictions. Filled squares (3C, 6C, and 12C) denote data used to fit the model and unfilled circles (0C and 9C) depict data used to validate the model predictions. Data for cases 0C (before 2 h) and 12C (all times) is adapted from ref 30. All other data was collected in this work. Note that the yield is dimensionless.

At each time, the yield, Y, was calculated as

$$Y(t) = \frac{[M_1^3(0)] - [M_1^3(t)] - [M_1^2(t)] - [M_1^1(t)] - [M_1^0(t)]}{[M_1^3(0)]}$$

This equation considers that all the nonfree monomers are incorporated into the product, as confirmed by the experimental ^{1}H nuclear magnetic resonance characterization in the work of Wang et al.[30] For fitting the kinetic parameters, the initial concentrations of the inhibitors I_1 and I_2 were taken to be 3, 6, and 12 times the initial concentration of M_1^3, in the simulations, to match the experimental conditions. We also carried out calculations for the 0C (no inhibitors) and 9C cases to understand the predictions of the model further and validate the rate constant parameters obtained. All the simulations were run until steady state was reached (24 h). The optimized values of all the parameters are summarized in Table 2.

Figure 2 depicts the yield vs time plots from our model, using the optimized set of rate constants. The corresponding experimental data is also shown. We found the root-mean-square deviation (RMSD) between the predicted and the experimental yield data to be 0.1107 for the fit data (3C, 6C, and 12C), indicating about 11% error in the predictions of the model, as compared to experimental data. Further, the RMSD for the validation cases (0C and 9C) was found to be 0.1073. Note that the same set of parameters is able to explain the

Table 2. Forward and Backward Rate Constants and Enhancement/De-Enhancement Factors Obtained by Fitting the Experimental Data to the Mechanistic Model[a]

RMSD	k_m (hr^{-1})	k_{mr} (hr^{-1})	k_i (hr^{-1})	k_{ir} (hr^{-1})	F_f	F_b
0.1107	302.125	4.456	1301.8	4.688	1.358	244.865

[a]The root-mean-square deviation (RMSD) between the model predictions and the experimental yield is also indicated.

https://doi.org/10.1021/jacsau.4c00077
JACS Au XXXX, XXX, XXX−XXX

experimental yield vs time plots at various inhibitor concentrations, indicating the robustness of the model to explain data under different experimental conditions. The discrepancy between the predicted and experimental yields for the 0C case at low times could be due to the lack of considering mass transfer limitations in the model. Further details about the data fitting procedure are given in the Methods section.

It is interesting to ask what happens if the inhibitor concentration is increased beyond the 12C case. As mentioned before, our previous work has shown that if the inhibitor-to-monomer concentration ratio (I/M) is increased beyond 12, the COF formation rate within 24 h is significantly reduced.[30] In the Supporting Information, Section S3, we present results for fitting the kinetic model using data for 15−24C cases. Therein, one sees that very high inhibitor concentrations could activate imine exchange with the COF, accelerating the inhibition of the sites in the polymer as well as the free reacting monomers. Indeed, we showed experimentally that the imine condensation product I_{12} could itself inhibit COF growth, as discussed earlier. This reaction is not considered in our model and could possibly explain the very low yield seen in those cases, which is much lower than what the kinetic model parameters listed in Table 1 would predict. Nevertheless, in the present model, the imine exchange is indirectly included via the composite reaction involving the decomposition of the imine and the reaction of the individual inhibitors with the growing 2D polymer, though this prevents the possibility of imine exchange being the dominant route due to a different (higher) rate constant.

KMC Simulations of the COF Growth Process

Next, we carried out KMC simulations to understand COF growth at the molecular level. We considered a graphene-like honeycomb lattice for the KMC simulations to account for the trifunctionality of the monomers. The lattice grid consisted of two triangular sublattices, wherein M_1 and I_1 can occupy the sites on one sublattice and M_2 and I_2 can attach on the other one due to the possible reactions between these species. Note that the stacking of COF layers is not considered in our model, which describes solely single-layer growth. To simplify the KMC algorithm, the first (inhibition of monomers) and the last (condensation of inhibitors) set of reactions were not carried out on the lattice but simply accounted for in terms of changes in the concentrations of the species involved in these reactions. In other words, these reactions do not change anything on the polymer lattice. The reaction rates were updated before each iteration of the simulation as the species concentration changes. For all the other sets of reactions which correspond to the COF growth, the lattice sites were updated according to the reaction picked by the algorithm. Following that, the concentrations of the species and the reaction rates were updated. Further details regarding the KMC algorithm are provided in the Methods section.

As the kinetic model developed above considers a well-mixed system, contrary to the localized phenomena modeled in KMC simulations, we found it essential to scale the corresponding parameters in the KMC simulations to obtain agreement with the experimental yield vs time plots. Indeed, the rate constant in the kinetic model is multiplied with a global species activity (the corresponding species concentration), whereas it is multiplied with a local species activity (unity) in the KMC simulations. Accordingly, the reaction rate constants obtained from the data fitting were scaled, as documented in Table 3. The backward reaction constant k_{mr} for the monomer detachment reactions was fixed to be zero to reduce the computational cost of the KMC simulations as it was found to be much smaller than the forward rate constants k_m and k_i (see Table 2). Future work can explore the effect of allowing monomer detachment in the KMC simulations. As the detachment of monomers is not allowed, the de-enhancement factor F_b was not used for the reaction rate calculations. Although the inhibitor detachment rate constant k_{ir} was found to be comparable to k_{mr}, this value was retained and not set to zero since the inhibitor concentrations are much larger than the monomer concentrations (3C, 6C, 9C, or 12C, for example).

Table 3. Scaled Forward and Backward Rate Constant Parameters and Enhancement Factor Used for the KMC Simulations of 2D COF Growth

RMSD	k_m (hr^{-1})	k_{mr} (hr^{-1})	k_i (hr^{-1})	k_{ir} (hr^{-1})	F_f
0.07	6042.492	0	1301.8	0.141	1.3585

In terms of specific changes, k_m was enhanced 20 times to achieve agreement with the experimental yield curves. The faster rate constant for polymerization required in KMC is because each local *uninhibited* polymer site participates in a reaction giving rise to a lower polymer activity, whereas in the kinetic model, all the polymer chains in the reaction mixture are lumped together, leading to a higher activity. Further, since we set k_{mr} to zero (as discussed above), we reduced k_{ir} by a factor of 0.03 to maintain parity between the low possibility of monomers and inhibitors detaching from the COF, as reflected by the comparable values of the rate constants k_{mr} and k_{ir} in Table 1. Note that it is sufficient to modify one of the rate constants among k_i and k_{ir} to vary the inhibitor attachment/detachment rate. We carried out a sensitivity analysis to demonstrate the robustness of the choices for k_m and k_{ir}, as documented in the Supporting Information, Section S4. Figure 3 presents the yield vs time plots obtained using the KMC simulations for the 0C, 3C, 6C, 9C, and 12C cases. The KMC yield curves show good agreement with the experimental data, except for the 0C case. The difference in the 0C case could be attributed to mass transport limitations in the experimental system which would slow down the rate of increase in yield with time, as compared to KMC simulation predictions. Note that a short induction period is seen in the experimental yield curve for the 12C case. As the KMC lattice is initiated with one COF seed, this induction period is not observed in our simulated yield curve.

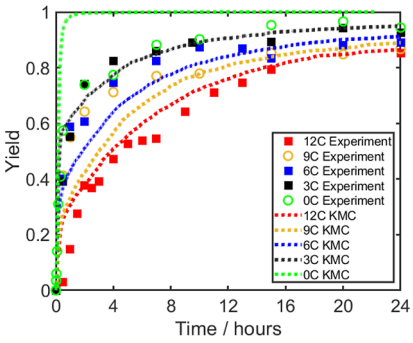

Figure 3. COF yield obtained from the KMC simulations, as a function of time, for different amounts of inhibitors in the system. The symbols represent the experimental data and the dotted lines represent the KMC predictions. The data points shown using filled squares are used in the RMSD calculation. Note that the yield is dimensionless.

https://doi.org/10.1021/jacsau.4c00077
JACS Au XXXX, XXX, XXX−XXX

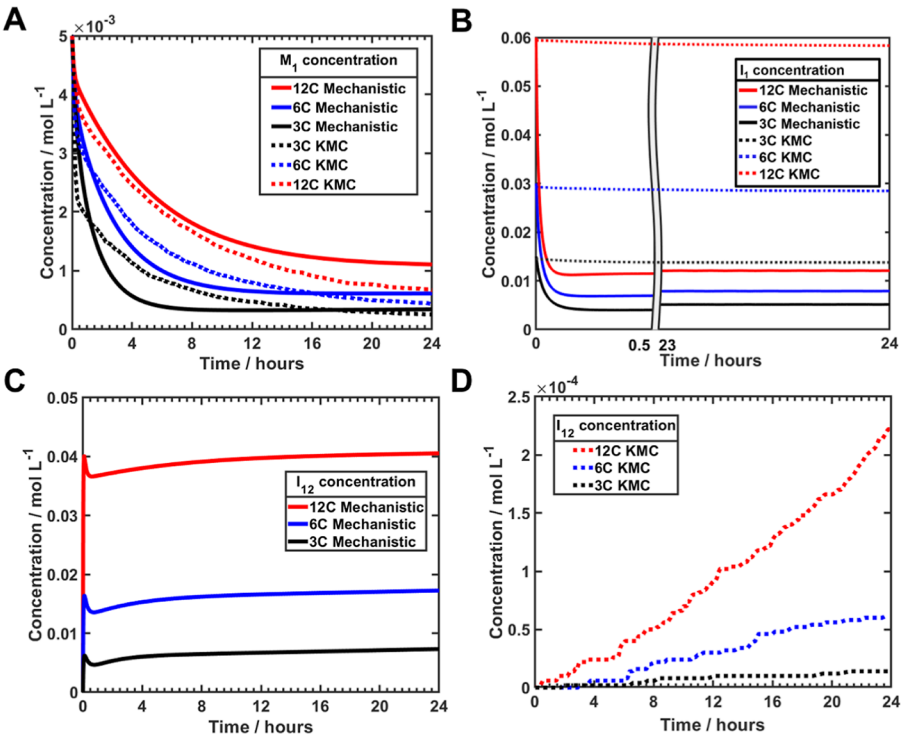

Figure 4. Concentration vs time plots for (A) monomer BTCA (M_1) using the mechanistic model and the KMC simulations, (B) inhibitor I_1 using both the methods, (C) imine product I_{12} using the mechanistic model, and (D) imine product I_{12} using the KMC simulations. Solid lines depict mechanistic model results and dotted lines represent the KMC results.

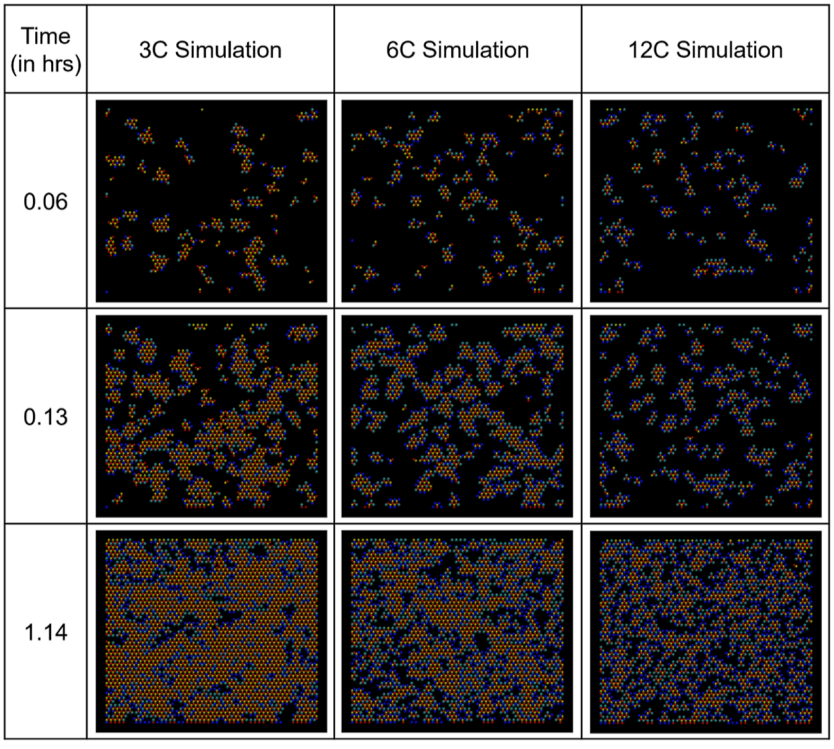

Figure 5. Time series of snapshots from the KMC simulations of COF growth for the 3C, 6C, and 12C cases at t = 0.06, 0.13, and 1.14 h.

To further understand the differences between the physics involved in the global kinetic model and the localized KMC simulations, in Figure 4, we present a comparison between the concentration vs time plots obtained using the mechanistic model and the KMC simulations for various species for the 3C, 6C, and 12C cases. The monomers are only consumed to form the polymer COF; thus, the monomer M_1 concentration vs time curve exhibits an opposite trend as that of the yield curve. Although the rate constants k_m and k_{ir} are scaled in the KMC simulations, the monomer concentration curves from the

https://doi.org/10.1021/jacsau.4c00077
JACS Au XXXX, XXX, XXX−XXX

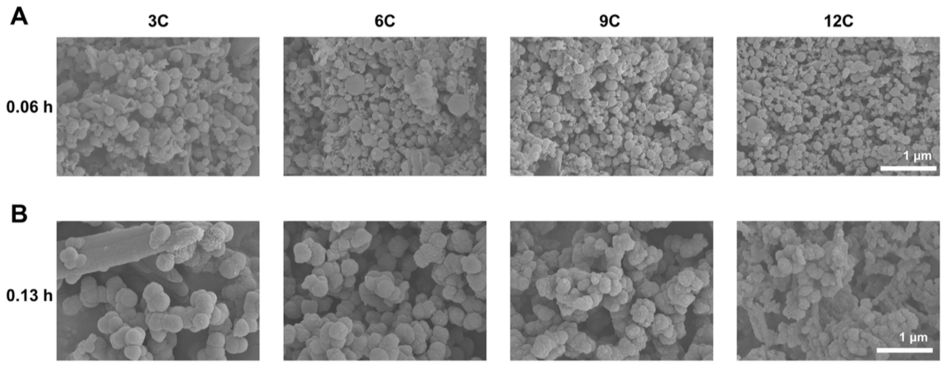

Figure 6. Morphology of the COF samples obtained using different amounts of inhibitors at (A) 0.06 h and (B) 0.13 h, captured using FESEM.

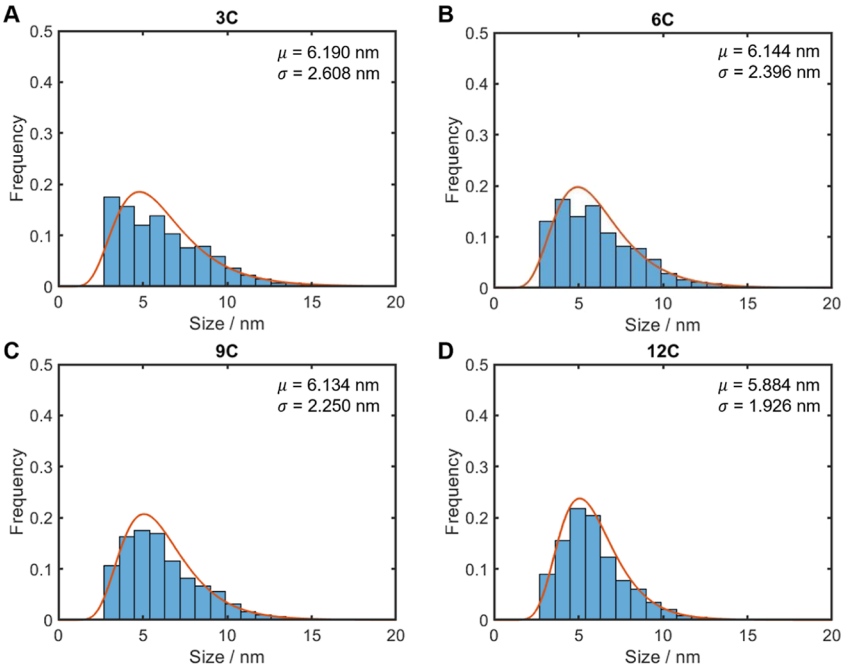

Figure 7. Flake size distribution at 0.06 h of reaction time obtained by averaging the results of 100 KMC simulation runs for different concentrations of inhibitors in the reaction system. The solid red lines indicate a fit to the log−normal distribution.

mechanistic model and KMC simulations qualitatively agree with each other, as shown in Figure 4A. Nevertheless, the concentration plots for the inhibitors show different behavior in the two models, as seen in Figure 4B. The mechanistic model predicts the consumption of a significantly larger amount of inhibitors as compared to the KMC simulations. As the COF growth is similar for the two methods, one explanation for different amounts of inhibitors being consumed could be the different amounts of imine I_{12} formed. To verify this, we plotted the imine product I_{12} concentration vs time, as shown in Figure 4C,D. The plots support the above argument as the I_{12} concentration is much higher in the mechanistic model as compared to the KMC simulations. Indeed, the reduction in the rate constant k_{ir} for the KMC simulation reduces the chances of free inhibitors being available to participate in the imine condensation reaction. Future studies could explore the use of different rate constants for the inhibitor addition to the monomer/COF and the inhibitor condensation reaction, along with the consideration of imine exchange, to better model the production of the imine.

Using KMC Simulations to Visualize the Growth of a COF Layer

We next analyzed the flake sizes in the COF network in the presence of varying inhibitor concentrations using KMC simulations. To this end, we present the snapshots of the KMC simulations to understand COF growth for the 3C, 6C, and 12C cases in Figure 5. At t = 0.06 h, we observed the least number of nucleates on the lattice sites for the 3C case. These nucleates were surrounded by a smaller number of inhibitors which is directly proportional to the initial inhibitor concentration. We saw a higher number of nucleates for the 12C case, but they were smaller in size as the inhibitors are more in number and thus attach at a faster rate to the COF than the monomers. Thus, as expected, the COF grew slowly in the 12C case when compared to the other two cases. At t = 0.13 h, we observed that the nucleates enlarged to form clusters in the 3C case, while the 6C simulation snapshot shows smaller clusters and the 12C case still has a large number of nucleates of very small size. This simulation prediction is in agreement with experimental microscopy images collected using field-emission scanning electron microscopy (FESEM), as shown in Figure 6. Indeed, therein one sees that the COF flake size follows the

https://doi.org/10.1021/jacsau.4c00077
JACS Au XXXX, XXX, XXX−XXX

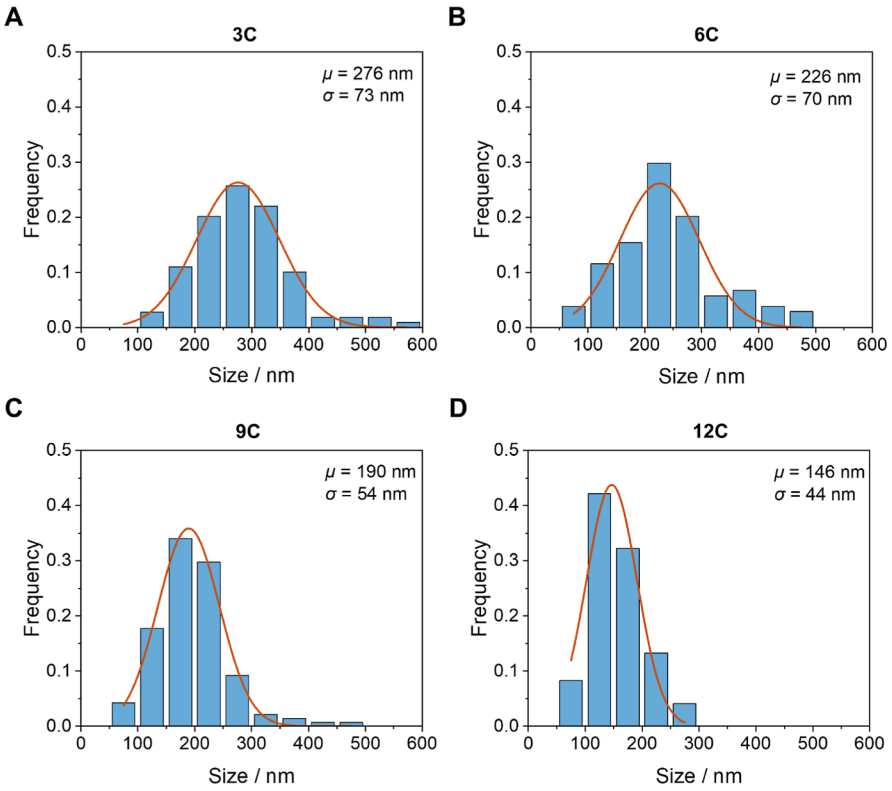

Figure 8. Particle size of the samples after 0.06 h of reaction with different dosages of competitors. The results shown are based on statistical analysis of more than 100 particles from the SEM images. The solid red lines indicate a fit to the normal distribution.

order 12C < 9C < 6C < 3C, which is also seen in the simulated flake sizes in Figure 5 for the 0.13 h case.

We also show KMC simulation snapshots at 4 and 24 h of simulation time in the Supporting Information, Section S5. It is evident in those snapshots that by 24 h, almost all the sites in the simulation box are occupied. However, more vacancies are found in the 12C case as the presence of a higher inhibitor concentration causes more sites to be blocked for polymer growth. Nevertheless, at sufficiently long periods of time (>72 h), crystalline structures are obtained in all cases, as seen experimentally.

These observations are further confirmed by our analysis of the flake size distribution at t = 0.06 h, as shown in Figure 7 for the KMC simulations (the flake size distribution at t = 0.13 h is shown in the Supporting Information, Section S6) and Figure 8 for the experiments. With an increase in the dosage of competitors, the COF flake size decreased gradually, and the size distribution became narrower, as seen in both Figures 7 and 8. Nevertheless, the COF obtained using a lesser amount of competitors, such as the 3C case, showed notable aggregation and fusion, resulting in some rods or flakes, as seen in Figure 6B. These irregular product particles further grew over time and even attached nanoflakes to their surface.[30] To verify this phenomenon with experiments, the product was dispersed in ethanol solvent by ultrasonication and detected using the dynamic light scattering (DLS) method, as shown in Section S7 in the Supporting Information. Therein, we indeed see larger flake sizes measured using DLS, indicating the fusion and aggregation of the COF flakes in solution.

It is noteworthy that the agreement between the flake size distributions in experiments and simulations is only qualitative. Moreover, at t = 1.14 h, all the three cases exhibited a single COF polymer in the KMC simulation with varying numbers of inhibitors blocking the monomer attachments. This is because our model is 2D in nature and does not capture the stacking of the nucleates in the third dimension. We did verify that increasing the simulation box size in the lateral direction does not affect the KMC simulation results, as seen in the Supporting Information, Section S8. The assumption of single-layer growth could be improved upon in future studies by investigating the stacking of the COF flakes. Nevertheless, as expected, the 12C case was found to have the lowest yield out of all the three cases in the simulations. Indeed, a higher inhibitor concentration slows down the kinetics of the COF growth to a larger extent due to the rapid attachment and detachment of the inhibitors. This leads to a controlled growth of the polymer and smaller sizes of the flakes in the COF, thus reducing defects and promoting self-repairing to obtain a higher-crystallinity structure.[41] Our work thus points to a trade-off in increasing the inhibitor concentration wherein one needs to optimize the inhibitor concentration to obtain the desired crystallinity while, at the same time, not decreasing the flake sizes significantly.

CONCLUSIONS

In this work, we developed a comprehensive model to study the kinetics of the reversible polycondensation termination reaction to synthesize COFs. To this end, we presented, for the first time, a generalized mechanistic theory, inspired by the Mayo−Lewis model of polymerization, to describe the controlled growth of COFs. We formulated a detailed set of reactions to model the complex chemistry occurring during COF growth in a generalized manner. As a first step, the mechanistic model was employed to obtain the rate constant values for the proposed system of reactions by fitting to experimental yield data. Further, we ran KMC simulations to understand the evolution of COF

https://doi.org/10.1021/jacsau.4c00077
JACS Au XXXX, XXX, XXX−XXX

structures with different numbers of inhibitors present in the reaction system. We demonstrated that the rate constant values need to be scaled before feeding them into the KMC simulations to reproduce the experimental yield data. We also concluded that the flake size in the COF is a function of the number of inhibitors present in the reaction system, unraveling an inhibitor concentration−flake size trade-off. Overall, the mechanistic model presented in this work allows the consideration of the effect of the functionalities of monomeric species on COF growth and enables the prediction of the growth rate and flake sizes as a function of the inhibitor concentration introduced in the reaction system. In the future, one could make the kinetic model more comprehensive by allowing for imine exchange reactions, considering the impact of water produced during condensation, and also allowing for reversible monomer attachment in the KMC simulations. To conclude, our model, fit using experimental kinetic data, can enable the controlled synthesis of 2D COFs in future studies by tuning the concentration of inhibitors to achieve the desired crystallinity and nanosheet size distribution, wherein higher crystallinity can be achieved using larger inhibitor concentrations and larger flakes can be achieved by using lower inhibitor concentrations.

EXPERIMENTAL AND COMPUTATIONAL METHODS

Materials

Benzaldehyde (98%), aniline (99.5%), and scandium(III) trifluoromethanesulfonate (Sc(OTf)3, 98%) were purchased from J&K Scientific Ltd. Further, 1,3,5-tris(4-aminophenyl)-benzene (TAPB, 98%) and 1,3,5-benzenetricarbaldehyde (BTCA, 98%) were purchased from Chemsoon Co., Ltd. In addition, hexane (AR) and 1,4-Dioxane (AR) were purchased from Sinopharm Chemical Reagent Co., Ltd. Finally, mesitylene (97%) was purchased from Shanghai Macklin Biochemical Co., Ltd.

Synthesis of TAPB-BTCA-COF Catalyzed by $Sc(OTf)_3$

Inhibitors I_1 (benzaldehyde) and I_2 (aniline) in 0−24 equiv (0−24C) were added to the reaction systems with TAPB and BTCA as monomers. In a typical experiment (12C), 17.6 mg of TAPB (0.05 mmol, 1 equiv) and 8.1 mg of BTCA (0.05 mmol) were dissolved in 10 mL of dioxane/mesitylene (1:2, v/v), followed by adding 60.7 μL of I_1 (0.6 mmol, 12 equiv) and 54.4 μL of I_2 (0.6 mmol, 12 equiv) to produce the reaction solution. $Sc(OTf)_3$ (0.73 mg, 1.5 μmol) in 0.1 mL of dioxane/mesitylene (2:1, v/v) was added to start the reaction. The reaction solution was filtered at different reaction times (from 0 to 24 h), and samples were collected at regular intervals. After drying at ambient conditions for 1 day naturally and under vacuum at 80 °C for another day, the mass of the sample was weighed, and the yield of the reaction was calculated using the formula

$$Y = \frac{m_{\text{weight}}}{(M_{\text{BTCA}} + M_{\text{TAPB}} - 3M_{\text{water}})n_{\text{monomer}}}$$

where m_{weight} is the measured mass of the synthesized COF, M_{BTCA} and M_{TAPB} are the molar masses of the two monomers, M_{water} is the molar mass of water, and n_{monomer} is the number of moles of one type of monomer added to the reaction mixture. Note that $(M_{\text{BTCA}} + M_{\text{TAPB}} - 3M_{\text{water}})n_{\text{monomer}}$ is the theoretical mass of the polymer formed assuming that all moles of monomer have reacted with the concomitant elimination of three moles of water and that the inhibitors were considered to be retained in the liquid phase.

Instrumentation for the Turbidity Measurements, FESEM, and DLS

The turbidity of the solutions was measured using a PERSEE TU-1901 UV spectrophotometer. The FESEM images were obtained using a Hitachi SU-8010 field-emission scanning electron microscope with an accelerating voltage of 3 kV. The samples were sprayed with Pt for 90 s for better electric conduction before carrying out FESEM imaging. Before each of the DLS measurements, 60 μL of the reaction solution obtained at 0.06 h was dispersed in 10 mL of ethanol by ultrasonication. Subsequently, DLS was performed using a Malvern Zetasizer Nano ZS90.

Kinetic Model

As discussed in the Results and Discussion section, we formulated a system of ordinary differential equations to describe the time evolution of the 17 species concentrations simultaneously. We also developed a function to solve this system of equations using the ode23 function in MATLAB R2022b for a given set of rate constants, thus predicting the yield of the COF growth process as a function of time. Subsequently, we used the nonlinear least-squares minimization function lsqnonlin to obtain the best-fit set of rate constants to obtain the maximum possible agreement between the predicted yield vs time curves and the corresponding experimental data. For this purpose, an error array was defined using the difference between the calculated yield and the experimental yield at various time points, and the sum of squared errors was minimized.

KMC Simulations

KMC simulations were carried out based on Gillespie's algorithm,[42] wherein the probability of a reaction being picked is proportional to the rate of that reaction.[43] This algorithm involves the generation of two uniformly distributed random numbers between 0 and 1, u_1 and u_2. The first random number is used to pick the reaction m as $\frac{\sum_{l=1}^{m-1} r_l}{r_{\text{net}}} < u_1 \leq \frac{\sum_{l=1}^{m} r_l}{r_{\text{net}}}$, where r_l denotes the rate of reaction l and r_{net} denotes the total rate, calculated as $r_{\text{net}} = \sum_{l=1}^{n} r_l$, and n denotes the total number of reactions. The second random number is used to update the simulation time as $t \rightarrow t + \frac{1}{r_{\text{net}}}\ln\left(\frac{1}{u_2}\right)$, where $\ln\left(\frac{1}{u_2}\right)$ converts the uniformly distributed random number u_2 to an exponentially distributed random number. Note that reaction types 4 through 7 were clubbed together while choosing the reaction that occurs (using u_1), and another uniformly distributed random number (u_3) was used to determine the exact reaction from those belonging to types 4 through 7. The simulation box used a 50 × 50 lattice in the lateral direction, leading to a total of 5000 sites considering both monomeric species, with a lattice constant of 18.72 Å and a lateral box area of 758810 Å^2. The vertical extent of the simulation box was calculated by using the initial concentration of monomers utilized in the experiments, i.e., 0.005 mmol/mL. Considering that equal numbers of monomers 1 and 2 correspond to the total number of lattice sites, i.e., 5000, the vertical length of the simulation box was calculated as the number of the monomer molecules (2500) divided by the initial concentration of monomers (0.005 mmol/mL), Avogadro's number, and the lateral area of the box, which gives a value of 1094 Å. Periodic boundary conditions were implemented for the lateral directions of the simulation box. The lattice was initiated with the smallest possible seed of the COF polymer, i.e., the moiety P_1^2−P_2^2. The reactions given in Table 1 were arranged into three sets which are different from the mechanistic model to efficiently implement the KMC algorithm. The first set consisted of reactions corresponding to inhibitors attaching to monomers and the condensation of inhibitors, which are reactions 1, 2, and 8 in Table 1. This approach is preferred as these reactions do not change anything on the lattice sites. The second set consisted of reaction 3, i.e., the coming together of two monomeric units on the COF lattice, as it is the most complicated one to implement. A "pairs list" was created to keep track of the number of occupied neighbors of each lattice site pair and the reaction rate corresponding to it. If any reaction from this set was picked, the pairs list was updated accordingly. Another list, called the "sites list", was created only for the occupied sites to keep track of whether their respective neighbor sites are unoccupied or occupied by a monomer or an inhibitor. For the sites occupied with a monomer, the reaction rate corresponding to it was taken to be zero as the detachment of monomers is not allowed in the KMC simulations. If a site is occupied by an inhibitor, it can be detached, and thus, the reaction rate

https://doi.org/10.1021/jacsau.4c00077
JACS Au XXXX, XXX, XXX−XXX

was stored accordingly. The third set of reactions corresponded to reactions involving the attachment of a sole monomer or inhibitor to the COF lattice. These include reactions 4 through 7 in Table 1 and can only occur for the empty sites which have a COF neighbor. At these empty sites, M_j^3, M_j^2, or M_j^1, where $j \in \{1,2\}$, can attach according to the number of unoccupied neighbors. The pairs list and sites list were both updated accordingly. Finally, after each iteration, the simulation time, the concentrations of the species, and the reaction rates were updated. To obtain the flake size distribution, we created an adjacency matrix for the 2D polymer and used the MATLAB function conncomp to identify the number of clusters (flakes) with different sizes. The equivalent circular diameter, based on the number of occupied polymer sites and the area of each site, was considered as the size of a given cluster. The fitdist and pdf functions were utilized to obtain the log−normal distribution curves for the flake size histogram plots.

■ ASSOCIATED CONTENT

Data Availability Statement

The MATLAB codes for the global kinetic model and local KMC simulations are available at https://github.com/agrgroup/COF_growth_model.

Supporting Information

The Supporting Information is available free of charge at https://pubs.acs.org/doi/10.1021/jacsau.4c00077.

Effects of different additives on COF synthesis, turbidity measurements for various inhibitor concentration cases, refitted model for I/M ratios higher than 12 and its implications, sensitivity analysis of the KMC simulation results using various sets of rate constant parameters to understand their influence on the model, snapshots of KMC simulations until 24 h, simulated flake size distribution at 0.13 h, DLS measurements of the flake sizes at 0.06 h, and sufficiency of the KMC box size (PDF)

■ AUTHOR INFORMATION

Corresponding Authors

Pingwei Liu − *State Key Lab of Chemical Engineering, College of Chemical and Biological Engineering, Zhejiang University, Hangzhou 310027, China; Institute of Zhejiang University − Quzhou, Quzhou 324000, China;* orcid.org/0000-0002-5060-0165; Email: liupingwei@zju.edu.cn

Ananth Govind Rajan − *Department of Chemical Engineering, Indian Institute of Science, Bengaluru, Karnataka 560012, India;* orcid.org/0000-0003-2462-0506; Email: ananthgr@iisc.ac.in

Authors

Shubhani Paliwal − *Department of Chemical Engineering, Indian Institute of Science, Bengaluru, Karnataka 560012, India; Department of Chemical Engineering, Imperial College London, South Kensington Campus, London SW7 2AZ, U.K.*

Wei Li − *State Key Lab of Chemical Engineering, College of Chemical and Biological Engineering, Zhejiang University, Hangzhou 310027, China; Institute of Zhejiang University − Quzhou, Quzhou 324000, China*

Complete contact information is available at: https://pubs.acs.org/10.1021/jacsau.4c00077

Author Contributions

⊥S.P. and W.L. contributed equally to this work.

Notes

The authors declare no competing financial interest.

■ ACKNOWLEDGMENTS

A.G.R. acknowledges financial support from the Department of Science and Technology (DST) and the Ministry of Electronics and Information Technology (MeitY) via the National Supercomputing Mission (NSM) under grant DST/NSM/R&D_HPC_Applications/Extension Grant/2023/16. A.G.R. also thanks the Infosys Foundation, Bengaluru, for an Infosys Young Investigator grant. P.L. acknowledges support from the National Natural Science Foundation of China (grants 21938010, 22293061, 22078289, 22078282, and 2197080461) and the Zhejiang Provincial Natural Science Foundation of China (grant LR20B060002).

■ REFERENCES

(1) Colson, J. W.; Dichtel, W. R. Rationally Synthesized Two-Dimensional Polymers. *Nat. Chem.* **2013**, *5* (6), 453−465.

(2) Zhang, G.; Zeng, Y.; Gordiichuk, P.; Strano, M. S. Chemical Kinetic Mechanisms and Scaling of Two-Dimensional Polymers via Irreversible Solution-Phase Reactions. *J. Chem. Phys.* **2021**, *154* (19), 194901.

(3) El-Kaderi, H. M.; Hunt, J. R.; Mendoza-Cortés, J. L.; Côté, A. P.; Taylor, R. E.; O'Keeffe, M.; Yaghi, O. M. Designed Synthesis of 3D Covalent Organic Frameworks. *Science* **2007**, *316* (5822), 268−272.

(4) Côté, A. P.; Benin, A. I.; Ockwig, N. W.; O'Keeffe, M.; Matzger, A. J.; Yaghi, O. M. Porous, Crystalline, Covalent Organic Frameworks. *Science* **2005**, *310* (5751), 1166−1170.

(5) Tran, M.; Kline, K.; Qin, Y.; Shen, Y.; Green, M. D.; Tongay, S. 2D Coordination Polymers: Design Guidelines and Materials Perspective. *Appl. Phys. Rev.* **2019**, *6* (4), 041311.

(6) Geng, K.; He, T.; Liu, R.; Dalapati, S.; Tan, K. T.; Li, Z.; Tao, S.; Gong, Y.; Jiang, Q.; Jiang, D. Covalent Organic Frameworks: Design, Synthesis, and Functions. *Chem. Rev.* **2020**, *120* (16), 8814−8933.

(7) Liao, Y.; Li, J.; Thomas, A. General Route to High Surface Area Covalent Organic Frameworks and Their Metal Oxide Composites as Magnetically Recoverable Adsorbents and for Energy Storage. *ACS Macro Lett.* **2017**, *6* (12), 1444−1450.

(8) Ascherl, L.; Sick, T.; Margraf, J. T.; Lapidus, S. H.; Calik, M.; Hettstedt, C.; Karaghiosoff, K.; Döblinger, M.; Clark, T.; Chapman, K. W.; Auras, F.; Bein, T. Molecular Docking Sites Designed for the Generation of Highly Crystalline Covalent Organic Frameworks. *Nat. Chem.* **2016**, *8* (4), 310−316.

(9) Huang, N.; Wang, P.; Jiang, D. Covalent Organic Frameworks: A Materials Platform for Structural and Functional Designs. *Nat. Rev. Mater.* **2016**, *1* (10), 16068.

(10) Liu, R.; Tan, K. T.; Gong, Y.; Chen, Y.; Li, Z.; Xie, S.; He, T.; Lu, Z.; Yang, H.; Jiang, D. Covalent Organic Frameworks: An Ideal Platform for Designing Ordered Materials and Advanced Applications. *Chem. Soc. Rev.* **2021**, *50* (1), 120−242.

(11) Zhao, X.; Pachfule, P.; Thomas, A. Covalent Organic Frameworks (COFs) for Electrochemical Applications. *Chem. Soc. Rev.* **2021**, *50* (12), 6871−6913.

(12) Ding, S.-Y.; Wang, W. Covalent Organic Frameworks (COFs): From Design to Applications. *Chem. Soc. Rev.* **2013**, *42* (2), 548−568.

(13) Wang, Z.; Zhang, S.; Chen, Y.; Zhang, Z.; Ma, S. Covalent Organic Frameworks for Separation Applications. *Chem. Soc. Rev.* **2020**, *49* (3), 708−735.

(14) Song, Y.; Sun, Q.; Aguila, B.; Ma, S. Opportunities of Covalent Organic Frameworks for Advanced Applications. *Adv. Sci.* **2019**, *6* (2), 1801410.

(15) Wu, M.-X.; Yang, Y.-W. Applications of Covalent Organic Frameworks (COFs): From Gas Storage and Separation to Drug Delivery. *Chin. Chem. Lett.* **2017**, *28* (6), 1135−1143.

(16) Zeng, Y.; Gordiichuk, P.; Ichihara, T.; Zhang, G.; Sandoz-Rosado, E.; Wetzel, E. D.; Tresback, J.; Yang, J.; Kozawa, D.; Yang, Z.; Kuehne, M.; Quien, M.; Yuan, Z.; Gong, X.; He, G.; Lundberg, D. J.; Liu, P.; Liu, A. T.; Yang, J. F.; Kulik, H. J.; Strano, M. S. Irreversible

Synthesis of an Ultrastrong Two-Dimensional Polymeric Material. *Nature* **2022**, *602* (7895), 91−95.
(17) Guo, J.; Jiang, D. Covalent Organic Frameworks for Heterogeneous Catalysis: Principle, Current Status, and Challenges. *ACS Cent. Sci.* **2020**, *6* (6), 869−879.
(18) Tao, S.; Jiang, D. Covalent Organic Frameworks for Energy Conversions: Current Status, Challenges, and Perspectives. *CCS Chem.* **2021**, *3*, 2003−2024.
(19) Zhou, Z.-W.; Cai, C.-X.; Xing, X.; Li, J.; Hu, Z.-E.; Xie, Z.-B.; Wang, N.; Yu, X.-Q. Magnetic COFs as Satisfactory Support for Lipase Immobilization and Recovery to Effectively Achieve the Production of Biodiesel by Maintenance of Enzyme Activity. *Biotechnol. Biofuels* **2021**, *14* (1), 156.
(20) Li, H.; Evans, A. M.; Castano, I.; Strauss, M. J.; Dichtel, W. R.; Bredas, J.-L. Nucleation-Elongation Dynamics of Two-Dimensional Covalent Organic Frameworks. *J. Am. Chem. Soc.* **2020**, *142* (3), 1367−1374.
(21) Li, H.; Chavez, A. D.; Li, H.; Li, H.; Dichtel, W. R.; Bredas, J.-L. Nucleation and Growth of Covalent Organic Frameworks from Solution: The Example of COF-5. *J. Am. Chem. Soc.* **2017**, *139* (45), 16310−16318.
(22) Li, H.; Evans, A. M.; Dichtel, W. R.; Bredas, J.-L. Quantitative Description of the Lateral Growth of Two-Dimensional Covalent Organic Frameworks Reveals Self-Templation Effects. *ACS Mater. Lett.* **2021**, *3* (4), 398−405.
(23) Castano, I.; Evans, A. M.; Li, H.; Vitaku, E.; Strauss, M. J.; Brédas, J. L.; Gianneschi, N. C.; Dichtel, W. R. Chemical Control over Nucleation and Anisotropic Growth of Two-Dimensional Covalent Organic Frameworks. *ACS Cent. Sci.* **2019**, *5* (11), 1892−1899.
(24) Li, Y.; Chen, W.; Xing, G.; Jiang, D.; Chen, L. New Synthetic Strategies toward Covalent Organic Frameworks. *Chem. Soc. Rev.* **2020**, *49* (10), 2852−2868.
(25) Evans, A. M.; Parent, L. R.; Flanders, N. C.; Bisbey, R. P.; Vitaku, E.; Kirschner, M. S.; Schaller, R. D.; Chen, L. X.; Gianneschi, N. C.; Dichtel, W. R. Seeded Growth of Single-Crystal Two-Dimensional Covalent Organic Frameworks. *Science* **2018**, *361* (6397), 52−57.
(26) Calik, M.; Sick, T.; Dogru, M.; Döblinger, M.; Datz, S.; Budde, H.; Hartschuh, A.; Auras, F.; Bein, T. From Highly Crystalline to Outer Surface-Functionalized Covalent Organic Frameworks—A Modulation Approach. *J. Am. Chem. Soc.* **2016**, *138* (4), 1234−1239.
(27) Baumgartner, B.; Bojdys, M. J.; Unterlass, M. M. Geomimetics for Green Polymer Synthesis: Highly Ordered Polyimides via Hydrothermal Techniques. *Polym. Chem.* **2014**, *5* (12), 3771−3776.
(28) Jin, Y.; Yu, C.; Denman, R. J.; Zhang, W. Recent Advances in Dynamic Covalent Chemistry. *Chem. Soc. Rev.* **2013**, *42* (16), 6634−6654.
(29) Smith, B. J.; Overholts, A. C.; Hwang, N.; Dichtel, W. R. Insight into the Crystallization of Amorphous Imine-Linked Polymer Networks to 2D Covalent Organic Frameworks. *Chem. Commun.* **2016**, *52* (18), 3690−3693.
(30) Wang, S.; Zhang, Z.; Zhang, H.; Rajan, A. G.; Xu, N.; Yang, Y.; Zeng, Y.; Liu, P.; Zhang, X.; Mao, Q.; He, Y.; Zhao, J.; Li, B.-G.; Strano, M. S.; Wang, W.-J. Reversible Polycondensation-Termination Growth of Covalent-Organic-Framework Spheres, Fibers, and Films. *Matter* **2019**, *1* (6), 1592−1605.
(31) Ma, T.; Kapustin, E. A.; Yin, S. X.; Liang, L.; Zhou, Z.; Niu, J.; Li, L. H.; Wang, Y.; Su, J.; Li, J.; Wang, X.; Wang, W. D.; Wang, W.; Sun, J.; Yaghi, O. M. Single-Crystal x-Ray Diffraction Structures of Covalent Organic Frameworks. *Science* **2018**, *361* (6397), 48−52.
(32) Lohse, M. S.; Bein, T. Covalent Organic Frameworks: Structures, Synthesis, and Applications. *Adv. Funct. Mater.* **2018**, *28* (33), 1705553.
(33) Waller, P. J.; Gándara, F.; Yaghi, O. M. Chemistry of Covalent Organic Frameworks. *Acc. Chem. Res.* **2015**, *48* (12), 3053−3063.
(34) Zhao, W.; Wang, T.-P.; Wu, J.-L.; Pan, R.-P.; Liu, X.-Y.; Liu, X.-K. Monolithic Covalent Organic Framework Aerogels through Framework Crystallization Induced Self-Assembly: Heading towards Framework Materials Synthesis over All Length Scales. *Chin. J. Polym. Sci.* **2019**, *37* (11), 1045−1052.
(35) Chen, X.; Xia, L.; Pan, R.; Liu, X. Covalent Organic Framework Mesocrystals through Dynamic Modulator Manipulated Mesoscale Self-Assembly of Imine Macrocycle Precursors. *J. Colloid Interface Sci.* **2020**, *568*, 76−80.
(36) Bhowmik, S.; Govind Rajan, A. Chemical Vapor Deposition of 2D Materials: A Review of Modeling, Simulation, and Machine Learning Studies. *iScience* **2022**, *25* (3), 103832.
(37) Govind Rajan, A.; Warner, J. H.; Blankschtein, D.; Strano, M. S. Generalized Mechanistic Model for the Chemical Vapor Deposition of 2D Transition Metal Dichalcogenide Monolayers. *ACS Nano* **2016**, *10* (4), 4330−4344.
(38) Nguyen, V.; Grünwald, M. Microscopic Origins of Poor Crystallinity in the Synthesis of Covalent Organic Framework COF-5. *J. Am. Chem. Soc.* **2018**, *140* (9), 3306−3311.
(39) Mayo, F. R.; Lewis, F. M. Copolymerization. I. A Basis for Comparing the Behavior of Monomers in Copolymerization; The Copolymerization of Styrene and Methyl Methacrylate. *J. Am. Chem. Soc.* **1944**, *66* (9), 1594−1601.
(40) Smith, B. J.; Dichtel, W. R. Mechanistic Studies of Two-Dimensional Covalent Organic Frameworks Rapidly Polymerized from Initially Homogenous Conditions. *J. Am. Chem. Soc.* **2014**, *136* (24), 8783−8789.
(41) Feriante, C.; Evans, A. M.; Jhulki, S.; Castano, I.; Strauss, M. J.; Barlow, S.; Dichtel, W. R.; Marder, S. R. New Mechanistic Insights into the Formation of Imine-Linked Two-Dimensional Covalent Organic Frameworks. *J. Am. Chem. Soc.* **2020**, *142* (43), 18637−18644.
(42) Gillespie, D. T. A General Method for Numerically Simulating the Stochastic Time Evolution of Coupled Chemical Reactions. *J. Comput. Phys.* **1976**, *22* (4), 403−434.
(43) Voter, A. F. Introduction to the Kinetic Monte Carlo method. In *Radiation Effects in Solids*; Sickafus Kurt, E., Kotomin, E. A., et al., Eds.; Springer Netherlands: Dordrecht, 2007; pp 1−23.

NOTE ADDED AFTER ASAP PUBLICATION

This paper published ASAP on May 31, 2024 with production errors in the text. The errors were corrected and the paper reposted on June 3, 2024.

https://doi.org/10.1021/jacsau.4c00077
JACS Au XXXX, XXX, XXX−XXX